Eur Biophys J (2012) 41:353–358
DOI 10.1007/s00249-012-0793-9

BIOPHYSICS LETTER

EBSA
Biophysics in Europe

Conformational switch of a flexible loop in human laminin receptor determines laminin-1 interaction

Carmen Di Giovanni · Alessandro Grottesi · Antonio Lavecchia

Received: 25 October 2011 / Revised: 10 January 2012 / Accepted: 16 January 2012 / Published online: 31 January 2012

Abstract The 37/67-kDa human laminin receptor (LamR) is a cell surface protein that interacts with molecules located in the extra-cellular matrix. In particular, interactions between LamR and laminins play a major role in mediating changes in the cellular environment that affect cell adhesion, neurite outgrowth, tumor growth and metastasis. The exact interaction mode of laminin-1 and LamR is not fully understood. Laminin-1 is thought to bind to LamR through interaction with the so-called peptide G (residues 161–180) and the C-terminal helix (residues 205–229). Here we performed 100-ns atomistic force field-based molecular dynamics simulations to explore the structure and dynamics of LamR related to laminin-1 interactions. Our main finding is that loop 188–197 in the C-terminal region is highly flexible. It undergoes a major change resulting in a conformational switch that partially solvent exposes the R180 residue in the final part of the G peptide. So, R180 could contribute to laminin-1 binding. Projection of the simulations along the first two principal components also confirms the importance of this conformational switch in the LamR. This may be a basic prerequisite to clarify the key structural determinants of the interaction of LamR with laminin-1.

Keywords Human laminin receptor · Molecular dynamics · Peptide G · Laminin-1 · Flexible loop

The authors Carmen Di Giovanni and Alessandro Grottesi have contributed equally to this study.

Electronic supplementary material The online version of this article (doi:10.1007/s00249-012-0793-9) contains supplementary material, which is available to authorized users.

C. Di Giovanni · A. Lavecchia (✉)
Department of Pharmaceutical and Toxicological Chemistry, "Drug Discovery Laboratory", University of Naples "Federico II", Via D. Montesano 49, 80131 Naples, Italy
e-mail: lavecchi@unina.it

A. Grottesi
Computational Medicine and Biology Group, CASPUR (Supercomputing Consortium for Applications for University and Research), Via dei Tizii 6, 00185 Rome, Italy

Introduction

In multicellular organisms, cells must be organized into tissues, organs and other structures. This is achieved through interactions between cells and extracellular matrices. Thus, it follows that there must be receptors on the surfaces of cells that recognize molecules in the extracellular matrix, bind to that matrix and transduce signals to the interior of the cell (Fatehullah et al. 2009). One such receptor is the human laminin receptor (LamR), which has a dual function as a component of the translational machinery and a cell surface receptor. At the cell surface, LamR exists as a monomer (37 kDa) and dimer (67 kDa). The relationship between the 37- and 67-kDa forms of LamR is not completely understood. The 67-kDa form is predicted to be a dimer, but whether LamR forms a homo-dimer or hetero-dimer has yet to be resolved (Venticinque et al. 2011). LamR can remodel laminin-1, a predominant protein of extracellular matrices, to alter tumor-cell gene expression and increase tumor aggressiveness, as well as alter intracellular signaling pathways (Berno et al. 2005). LamR is therefore considered a useful prognostic marker for determining the severity of tumors (Ménard et al. 1998). Further, LamR, which is upregulated in a number of human cancers, plays a role in migration, tumor invasion and metastasis through interactions with laminin-1 (Ménard et al. 1998; Wewer et al. 1987). Laminin-1, a 900-kDa glycoprotein,

contains many bioactive domains involved in binding both integrin and nonintegrin receptors, and is vital for basement membrane assembly. Mapping the LamR binding sites for laminin-1 may therefore contribute to the development of drugs that inhibit LamR interactions with laminin-1 and aid in the prevention of tumor growth and metastasis (Fatehullah et al. 2009).

Recently, the structure of the 37-kDa LamR precursor (fragment 1–205) was solved at 2.15 Å resolution (Jamieson et al. 2008) (Supplementary Material, Fig. S1A). The precise contact sites between LamR and laminin-1 are partially known. One of the possible interactions involves a nonapeptide from the β1 chain of laminin-1 (CDPGYIGSR) and residues 205–229 (RDPEEIEKEEQAAAEKAVTKEE FQG) of LamR (Kazmin et al. 2000; Starkey et al. 1999). These residues are predicted to adopt a mainly helical secondary structure, presenting two faces: a highly charged polar heparan-sulfate-binding surface and a more hydrophobic surface that interacts with laminin-1 (Kazmin et al. 2000). The LamR crystal structure starts at residue Q9 and finishes at residue R205, with almost all of the C-terminal laminin-binding site missing (not present in the prokaryotic and lower eukaryotic ribosomal proteins). An additional LamR binding site that binds laminin-1 with high affinity ($K_d = 51.8$ nM) is the so-called peptide G (residues 161–180, IPCNNKGAHSVGLMWWMLAR), which contains the palindromic sequence LMWWML (Castronovo et al. 1991; Magnifico et al. 1996; Taraboletti et al. 1993) and was shown to bind laminin-1, to inhibit binding of tumor cells to endothelial cells and to increase the metastases of human melanoma cells in nude mice (Castronovo et al. 1991; Magnifico et al. 1996; Taraboletti et al. 1993). In addition, peptide G increases and stabilizes the binding of laminin-1 on tumor cells (Magnifico et al. 1996).

LamR crystal structure reveals that almost all the G peptide is solvent buried by a surface flexible loop (residues 188–197), flanked by a C-terminus α-helix (residues 198–204), making it partially inaccessible to binding of laminin-1 (Supplementary Material, Fig. S1A). Of the peptide G segment, only residues 166 and 169 are solvent accessible in the LamR crystal structure. Mutagenesis studies (Jamieson et al. 2011) revealed that the K166A mutant does not affect laminin binding, suggesting that K166 is not essential for the laminin-binding function of LamR. In addition, several authors hypothesized that major conformational changes are required to enable laminin-1 binding to LamR (Fatehullah et al. 2009; Nelson et al. 2008). Moreover, Jamieson et al. (2011) described an additional laminin binding site on LamR, comprising residues F32, E35 and R155. Some mutations of these residues have been reported to determine a significant loss of laminin-1 binding. So, to date, the key determinants of the laminin-1/LamR interaction are not completely understood.

The purpose of this work was to study the conformation dynamics of the LamR structure by means of molecular dynamics (MD) simulations to improve the understanding of the molecular basis of its interaction with laminin-1.

Methods

Molecular dynamics simulations

All simulations performed here were based on a slight modification of the protocol used in Labro et al. (2008). Briefly, we ran all simulations using GROMACS v.4.5.3 with the GROMOS96 force field (Van Gunsteren et al. 1996) in the NVT ensemble at constant volume and temperature, with periodic boundary conditions. Initial velocities were taken from a Maxwell-Boltzmann distribution at the desired temperature. The whole system (protein, solvent and ions) was coupled to an external thermostat using the V-Rescale algorithm (Bussi et al. 2007). Long-range electrostatic interactions were calculated using the particle mesh Ewald method, with a 1.2-nm cutoff for the real space calculation. A cutoff radius of 1.2 nm was used for the van der Waals interactions. The LINCS algorithm was used to constrain bond lengths, and the time step for integration was 2 fs.

System setup

The initial protein coordinates (PDB code: 3BCH) were taken from PDB (4). All ionizable groups were assigned their default state at pH = 7. The total protein charge was −4, and counter ions were added to neutralize simulation cells accordingly. All energy minimization procedures used 1,000 steps of the steepest descent method to relax any steric conflicts generated during system setup. In order to further equilibrate the solvent was energy minimized and equilibrated; then the whole system was warmed up in a stepwise manner: five short time scale unrestrained MD runs (typically 50 ps) were performed at 50, 100, 200, and 250 K to bring the whole system to 300 K. Two independent simulations were performed with different initial velocities at 300 K. The total simulation time for each trajectory was 100 ns.

Analysis

All analyses were performed using GROMACS and/or an in-house locally written code. Simulations were analyzed by means of principal component analysis (PCA). This technique relies on calculation of the positional fluctuation covariance matrix of protein Cα atoms, and its diagonalization enables detection of the large-amplitude motions

that best characterize protein dynamics (Amadei et al. 1993; Garcia 1992). In order to detect dominant concerted motions in LamR, all trajectories were projected along selected eigenvectors. To detect H-bonds in the LamR structure during the simulation, we used a donor–acceptor distance smaller than 0.35 nm and an acceptor–donor-hydrogen cutoff angle equal to 30 degrees. Secondary structure content and solvent accessible surface area were calculated using DSSP (Kabsch and Sander 1983). The VMD software (Humphrey et al. 1996) was extensively used for visualizations and the preparation of structural diagrams presented in this study. We performed two distinct simulations (100 ns each) of the LamR in solution at 300 K using a different set of initial velocities. The rationale was to increase the statistical significance of the measured results and to limit the insufficient sampling that inevitably affects MD simulations. In order to assess the convergence of the sampled motion of LamR on the simulation time, we carried out a time-averaged block analysis of the mean square fluctuations of the Cα atoms in the α-helical segments of the protein (Faraldo-Gómez et al. 2004). More details are provided in the Supplementary Materials of this manuscript.

Results and discussion

To measure the extent of conformational drift during the course of the simulations for LamR, we measured the root mean square deviation (RMSD) of the Cα carbon atoms with respect to the initial minimized X-ray structure (Fig. 1). In all simulations performed we found a major RMSD change that took place after a few tens of nanoseconds with a range from 0.2 to a final 0.4 nm. To determine the protein regions that mainly contributed to this conformational trend, we also calculated the RMSD only over the residue range 9–187 (Supplementary Material, Fig. S1B) and found that actually the region spanning the 188–204 residues of LamR gives the main contribution to the RMSD change. To get a more detailed picture of the protein regions involved, we calculated the Cα root mean square fluctuations (RMSF) with respect to their average position in the trajectory: the chain flexibility of the 188–197 loop is actually much higher compared to the flanking residues and to the whole protein. This may reflect the flexible nature of the loop (188–197) in LamR. To show this further, we calculated the RMSF either in the 5–100 (Supplementary Material, Fig. S2, black line) or in the 12–100 ns range (Fig. S2, red line). The data confirmed that the loop 188–197 is the most flexible element of LamR responsible for the RMSD change measured in all simulations. The initial part of the C-terminal (residues 198–205) was not involved in the conformational change

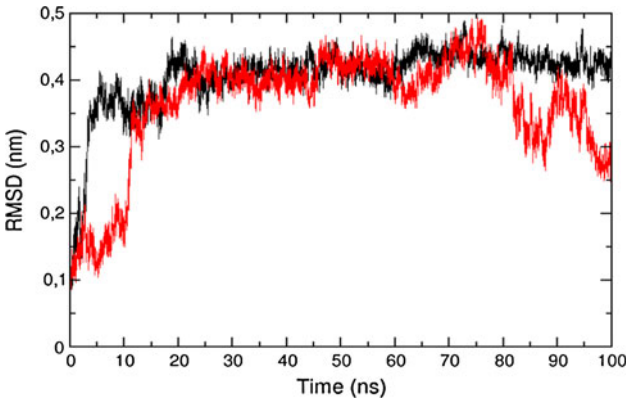

Fig. 1 Root mean square deviation of the Cα atoms position of LamR with respect to the initial X-ray minimized structure. The *black* and *red* plot refers to two independent simulations performed with different initial velocities at 300 K. A major drift is observed in both cases involving the C-terminal loop (see text for details)

observed, as the secondary structure analysis (Supplementary Material, Fig. S3) showed that the integrity of the α-helix in the residue range 199–204 is retained. A more quantitative estimate of protein mobility and simulation convergence was performed by means of block analysis of the mean square fluctuations (MSF) of the α-helical Cα atoms with respect to their average position. Figure S4 of the Supplementary Material shows that full convergence of the secondary structure flexibility is obtained at 5,000 ps time windows, suggesting that the protein dynamics of the secondary structures are sufficiently sampled at the 100-ns time scale.

We identified a key H-bond, present in the X-ray structure, holding the flexible loop and the peptide G tightly bound to each other. As shown in Fig. 2, the donor-acceptor H-bond distance between W176 (side chain $N^{\varepsilon 1}$), located on the peptide G, and V197 (main chain O), located on the flexible loop, is highly variable. In particular, the

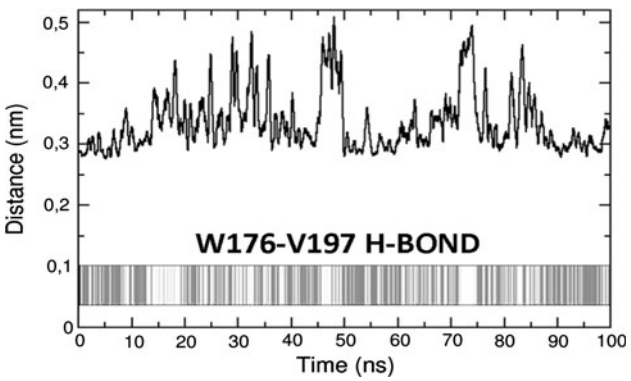

Fig. 2 Donor-acceptor distance of the H-bond involving W176 ($N^{\varepsilon 1}$) and V197 (main chain oxygen O). The occurrence of the W176-V197 H-bond as a function of simulation time is also reported as a *dark-gray band* at the bottom

donor-acceptor average distance at the end of the simulation (last 5 ns: 0.34 ± 0.03) is higher than the starting value (0.27 nm). We hypothesize that breaking of this important interaction may be correlated to exposure of the last residue of peptide G to the bulk solvent. To show this, we measured the instantaneous exposure of peptide G residues at different time frames during all simulations and found that only R180 (which is fully buried in the initial crystal structure, with a SASA of 9 $Å^2$) becomes partly exposed with final SASA of 47 $Å^2$ after 80 ns (Supplementary Material, Fig. S5).

What is the nature of the molecular mechanism underlying the conformational switch of the flexible loop? To answer this, we performed a principal components analysis as described in "Methods." Accordingly, the intra-molecular motions of LamR can be described by projecting the trajectory data onto the first and second principal components (that account for 30 and 17% of total protein Cα fluctuations, respectively). In the first eigenvector (Fig. 3a) the LamR trajectory projection is associated with two distinct conformations of the flexible loop: a closed and an open one, characterized by the partial exposure of peptide G to the bulk solvent. The normalized distribution of eigenvector projections highlights this scenario (Fig. 3b) of two states of the loop. We hypothesized that these closed and open conformations were correlated to the presence of salt bridges between ionic pairs. To show this, we measured the center-of-mass (COM) distances of E192-R184 and E192-K11 (Fig. 4), and the data showed that this distance is below 1 nm when the flexible loop is closed (and eventually it lowers down to 0.5 nm, where a salt bridge is actually formed) and jumps to 2 nm or higher when the loop conformation is switched to its open state after approximately 70 ns. The second eigenvector (which accounts for 17% of total protein fluctuations) (Fig. 5) describes the molecular event associated with the backward motion of the flexible loop to its X-ray-like conformation ($\sim$100 ns). In particular, we measured the formation of a transient salt bridge between K11 and D200. As shown in Fig. 5, the COM distance drops to 0.5 nm in the time range between 70 and 80 ns, suggesting a correlation between this event and the overall C-terminal loop conformational change. The whole dynamic process of the flexible loop motion together with the transient formation of the K11-D220 salt bridge can be observed in Fig. 4B (snapshot of the LamR conformation taken at 75 ns in the bottom panel) and in the movie M1 (see Supplementary Material).

In view of the difficulty of specifically targeting the peptide G/laminin-1 binding site, attention has turned in recent years to alternative regions in the protein. One strategy focuses on identifying single amino acids that are critical for the LamR substrate interaction at protein-protein interfaces. In this regard, eight residues were selected by Jamieson et al. (2011) based on their proximity to the canonical peptide G binding site and their conservation in the LamR family. Site-directed mutagenesis was used to determine the importance of each of the residues for lamin-1 interaction. Strong mutations of F32V, E35K and R155A resulted in loss of migration inhibition, showing their involvement in laminin-1 binding. During MD simulations, these latter residues (see Supplementary Movie M2) kept their solvent exposed position in the protein structure and did not undergo significant conformational changes. This fits with their supposed role as potential binding hotspot

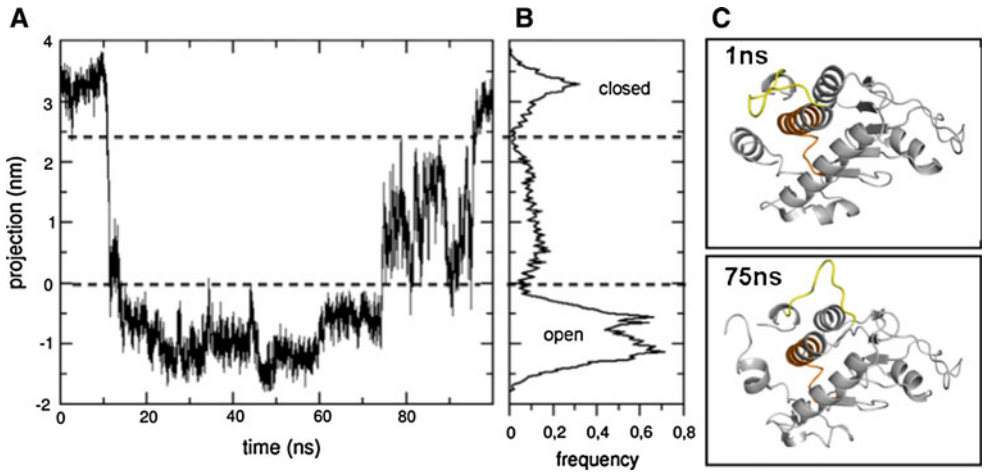

Fig. 3 **a** Projection of the Cα atom's trajectory onto the first principal component of the positional fluctuation covariance matrix as a function of simulation time. **b** The normalized frequency distribution of the measured projection is shown as a function of the projection along the principal components. *Dashed line* marks transitions between closed and open conformation of the flexible loop. **c** Snapshots of the LamR structure conformation showing the loop in the closed (*top*) and open (*bottom*) state, taken at 1 and 75 ns, respectively. Peptide G and flexible loop are *highlighted* in *orange* and *yellow*, respectively

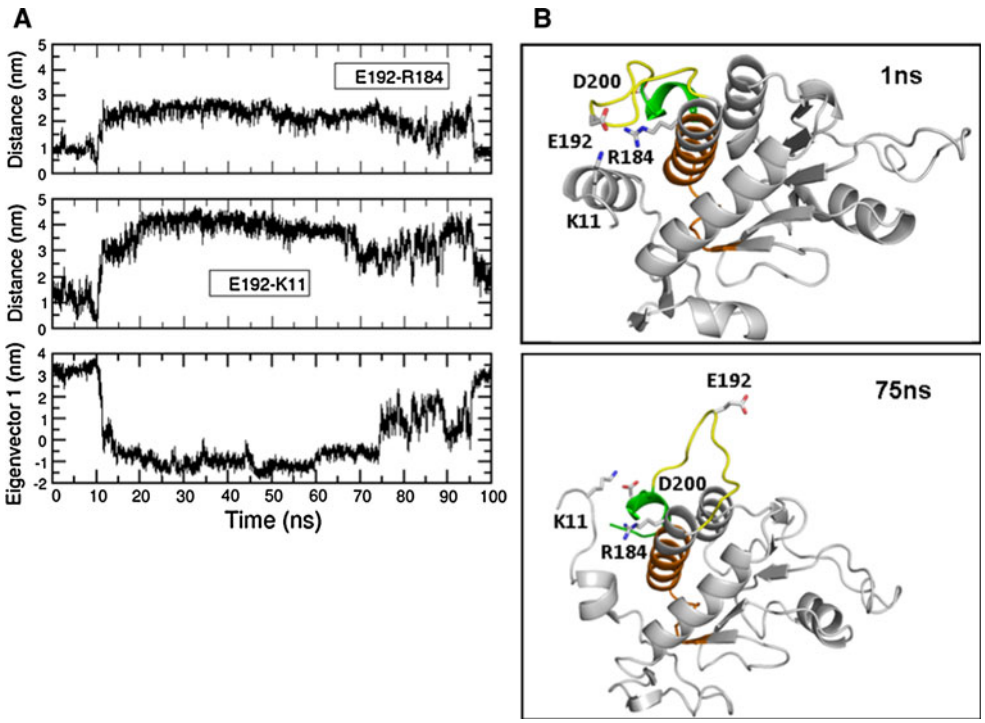

Fig. 4 **a** Ion pair distance between E192 and R184 (*top panel*) and E192 and K11 (*middle panel*) versus time; the projection of the Cα atoms of the trajectory along the first eigenvector is shown in the *bottom panel*. **b** LamR conformation after 1 ns (*top*) viewing the E192-R184 and E192-K11 salt bridges with the flexible loop in the closed conformation; LamR conformation in the open state, taken at 75 ns (*bottom*). Peptide G, flexible loop and C-terminal α-helix are *highlighted* in *orange*, *yellow* and *green*, respectively

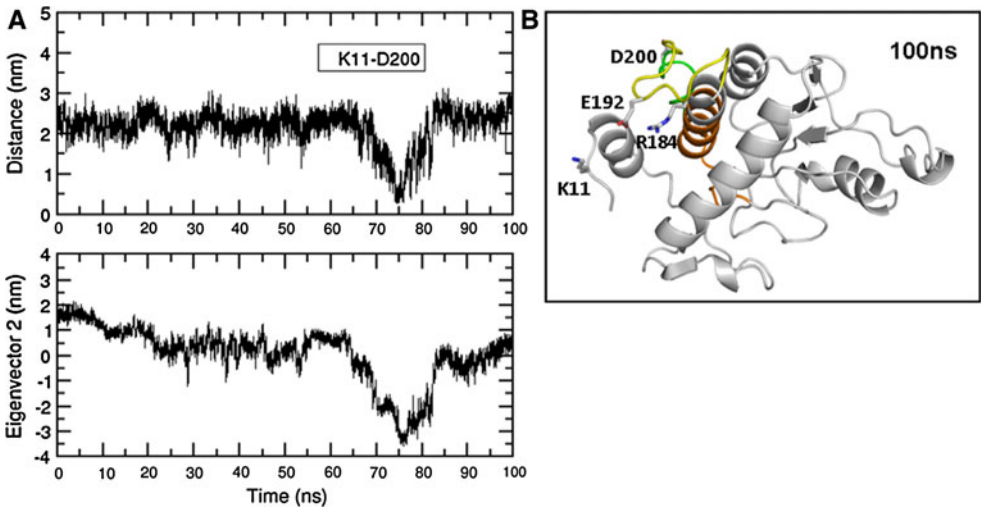

Fig. 5 **a** *Top panel* ion pair distance of the K11-D200 salt bridge as a function of simulation time calculated on simulation run 2; (**a**, *bottom panel*): projection of the Cα atoms trajectory of LamR (run 2) along the second principal component of the fluctuations covariance matrix (see "Methods"). **b** Snapshot of the LamR structure taken at 100 ns. It describes the backward motion of the flexible loop to its X-ray-like conformation. Peptide G, flexible loop and C-terminal α-helix are *highlighted* in *orange*, *yellow* and *green*, respectively

residues that mediate substrate laminin-1 recognition. However, other experimental information about the sequence of laminin-1 recognized from this LamR region could be useful to corroborate this hypothesis. Moreover, in the same paper, Jamieson et al. (2011) reported that mutation of K166 to alanine did not affect laminin-1 binding, suggesting that K166 is not essential for laminin-1 binding of LamR. Our data suggest that the interaction regions of laminin-1/peptide G are rather small and bordered by few hotspot residues on peptide G. Indeed, after extensive MD simulations, the only residue that become partly solvent exposed is R180, while almost all the peptide G is kept buried with the exception of H169, which retains its solvent exposed position (see Fig. S1 in the Supplementary Material) without substantial conformational changes. Therefore, R180 represents a new potential residue contributing to binding of laminin-1.

It should be emphasized that the LamR structure used in this study lacks almost all of the C-terminal domain (205–229), which extensively supplies the laminin-1 binding (Landowski et al. 1995; Castronovo et al. 1991; Wang et al. 1992; Wewer et al. 1987; Kazmin et al. 2000; Jamieson et al. 2011). Based on this, a successive step will be to study the conformational dynamics of LamR including the full C-terminal tail alone and in complex with the laminin-1 $\beta 1$ nonapeptide.

This work represents a basic prerequisite to deriving the key structural determinants of LamR/laminin-1 interaction. It can also provide the basis for establishing new potential binding regions for the design of small molecule inhibitors of LamR that are useful for the prevention of tumor growth and metastasis.

References

Amadei A, Linssen ABM, Berendsen HJC (1993) Essential dynamics of proteins. Proteins 17:412–425

Berno V, Porrini D, Balsari A, Ménard S, Tagliabue E (2005) The 67 kDa laminin receptor increases tumor aggressiveness by remodeling laminin-1. Endocr Relat Cancer 12:393–406

Bussi G, Donadio D, Parrinello M (2007) Canonical sampling through velocity rescaling. J Chem Phys 126:014101

Castronovo V, Taraboletti G, Sobel ME (1991) Functional domains of the 67-kDa laminin receptor precursor. J Biol Chem 266:20440–20446

Faraldo-Gómez JD, Forrest LR, Baaden M, Bond PJ, Domene C, Patargias G, Cuthbertson J, Sansom MSP (2004) Conformational sampling and dynamics of membrane proteins from 10-nanosecond computer simulations. Protein Struct Func Bioinf 57:783–791

Fatehullah A, Doherty C, Pivato G, Allen G, Devine L, Nelson J, Timson DJ (2009) Interactions of the 67 kDa laminin receptor and its precursor with laminin. Biosci Rep 30:73–79

Garcia AE (1992) Large-amplitude nonlinear motions. Protein Phys Rev Lett 68:2696–2699

Humphrey W, Dalke A, Schulten K (1996) VMD: visual molecular dynamics. J Molec Graph 14:33–38

Jamieson KV, Wu J, Hubbard SR, Meruelo D (2008) Crystal structure of the human laminin receptor precursor. J Biol Chem 283:3002–3005

Jamieson KV, Hubbard SR, Meruelo D (2011) Structure-guided identification of a laminin binding site on the laminin receptor precursor. J Mol Biol 405:24–32

Kabsch W, Sander C (1983) Dictionary of protein secondary structure: pattern recognition of hydrogen-bonded and geometrical features. Biopolymers 22:2577–2637

Kazmin DA, Hoyt TR et al (2000) Phage display mapping for peptide 11 sensitive sequences binding to laminin-1. J Mol Biol 298:431–445

Labro AJ, Grottesi A, Sansom MS, Raes AL, Snyders DJ (2008) A Kv channel with an altered activation gate sequence displays both "fast" and "slow" activation kinetics. Am J Physiol Cell Physiol 294:C1476–C1484

Landowski TH, Selvanayagam U, Starkey JR (1995) Control pathways of the 67 kDa laminin binding protein: surface expression and activity of a new ligand binding domain. Clin Exp Metastasis 13:357–372

Magnifico A, Tagliabue E et al (1996) Peptide G, containing the binding site of the 67-kDa laminin receptor, increases and stabilizes laminin binding to cancer cells. J Biol Chem 271:31179–31184

Ménard S, Tagliabue E, Colnaghi MI (1998) The 67 kDa laminin receptor as a prognostic factor in human cancer. Breast Cancer Res Treat 52:137–145

Nelson J, McFerran NV et al (2008) The 67 kDa laminin receptor: structure, function and role in disease. Biosci Rep 28:33–48

Starkey JR, Uthayakumar S, Berglund DL (1999) Cell surface and substrate distribution of the 67-kDa laminin-binding protein determined by using a ligand photoaffinity probe. Cytometry 35:37–47

Taraboletti G, Belotti D et al (1993) Enhancement of metastatic potential of murine and human melanoma cells by laminin receptor peptide G: attachment of cancer cells to subendothelial matrix as a pathway for haematogenous metastasis. J Natl Cancer Inst 85:235–240

van Gunsteren WF, Billeter SR, Eising AA, Hünenberger PH, Krüger P, Mark AE, Scott WRP, Tironi IG (1996) Biomolecular simulation: the GROMOS96 manual and user guide. vdf Hochschulverlag AG an der ETH Zürich and BIOMOS b.v. Zürich, Groningen

Venticinque L, Kelly V, Jamieson J, Meruelo D (2011) Interactions between laminin receptor and the cytoskeleton during translation and cell motility. PLoS One 6:e15895

Wang K-S, Kuhn RJ, Strauss EG, Ou S, Strauss JH (1992) High-affinity laminin receptor is a receptor for Sindbis virus in mammalian cells. J Virol 66:4992–5001

Wewer UM, Taraboletti G, Liotta LA et al (1987) Role of laminin receptor in tumor cell migration. Cancer Res 47:5691–5698